The Astrophysical Journal, 653:490–502, 2006 December 10

PREMAXIMUM SPECTROPOLARIMETRY OF THE TYPE Ia SN 2004dt[1]

Lifan Wang,[2,3,4] Dietrich Baade,[5] Peter Höflich,[6] J. Craig Wheeler,[6] Koji Kawabata,[7]
Alexei Khokhlov,[8] Ken'ichi Nomoto,[9] and Ferdinando Patat[5]
Received 2004 September 24; accepted 2006 July 29

ABSTRACT

We report observations of SN 2004dt obtained with the Very Large Telescope (VLT) of the European Southern Observatory (ESO) on 2004 August 13.30, when the supernova was more than a week before optical maximum. SN 2004dt showed strong lines of O I, Mg II, Si II, and Ca II, with typical velocities of absorption minimum around 17,000 km s^{-1}. The line profiles show material moving at velocities as high as 25,000 km s^{-1} in these lines. The observations also reveal absorption lines from S II and Si III with a velocity of only 11,000 km s^{-1}. The highest velocity in the S II features can be traced to about 15,000 km s^{-1}, much lower than those of O, Mg, Si, and Ca. SN 2004dt has a polarization spectrum unlike any previously observed. The variation of the polarization across some Si II lines approaches 2%, making SN 2004dt the most highly polarized SN Ia ever observed. In contrast, the strong line of O I at 777.4 nm shows little or no polarization signature. The degree of polarization points to a silicon layer with substantial departure from spherical symmetry. A geometry that would account for the observations is one in which the distribution of oxygen is essentially spherically symmetric, but with protrusions of intermediate-mass elements within the oxygen-rich region.

Subject headings: supernovae: individual (SN 2004dt) — techniques: polarimetric

1. INTRODUCTION

As for core-collapse supernovae, high-quality spectropolarimetry of Type Ia supernovae (SNe Ia) is revealing a complex array of behavior that has opened a new window of exploration of this class of explosions (Wang et al. 1996, 1997, 2003b, 2004; Howell et al. 2001). While there are indications that the degree of polarization of core-collapse supernovae increases with time after explosion (Wang et al. 2001, 2002; Leonard et al. 2001), the time evolution of Type Ia supernovae seems to be rather different (Wang 2003).

Polarimetry of SN Ia shows that the degree of polarization of normal SN Ia is $\lesssim 0.3\%$, which is much lower than the typical polarization of core-collapse supernovae (Wang et al. 1996). Spectropolarimetry of the normally bright SN 1996X at optical maximum tentatively showed intrinsic polarization of about 0.3%, which implies geometrical asphericities of about 10% (Wang et al. 1997). Hydrodynamic instabilities just beyond the layers of complete thermonuclear equilibrium may have contributed to the polarization signal from SN 1996X. Howell et al. (2001) showed that SN 1999by, a subluminous SN Ia, was polarized at a level of 0.7% in the red continuum.

The observations of the normally bright SN 2001el revealed the geometric structure of an SN Ia in different chemical layers. The degree of polarization showed significant time evolution (Wang et al. 2003b). An exceedingly strong Ca II feature at velocity of 20,000–26,000 km s^{-1} was highly polarized. This feature showed that the outermost layers of the supernova ejecta had a highly aspherical geometry (Wang et al. 2003b; Kasen et al. 2003). Deeper inside the ejecta, the silicon-rich layer also displayed asphericity as evidenced by the detection of polarization of $\sim 0.3\%$ for the Si II 635.5 nm line. When the photosphere receded deep inside the iron-rich layers, the polarization diminished and the supernova appeared spherical. Wang et al. (2003b) listed several possible origins of this asymmetric high-velocity material: matter from a disk or companion star that is swept up by the supernova ejecta; newly synthesized material produced by thermonuclear reactions in the high-velocity collision between supernova ejecta and the surroundings; and a clump of matter ejected from the intrinsic thermonuclear combustion process. Gerardy et al. (2004) examined the high-velocity Ca II feature in SN 2003du[10] and concluded that the strength of the Ca II in that event was consistent with solar abundance of calcium in a hydrogen plasma (that the bulk of the matter was helium or carbon/oxygen cannot be ruled out) that was swept up from distances consistent with the expected separation of the companion star.

We present in this paper observations of SN 2004dt. This event showed exceptionally strong and broad lines of Si II and O I, and revealed the strongest polarization signal we have yet measured for a SN Ia. The discovery and premaximum observations are described in § 2; the spectral and spectropolarimetry features and their implications for ejecta geometry are discussed in § 3. The inferred ejecta geometry is given in § 4. The observations of SN 2004dt are compared to other SN Ia in § 5. Comments on theoretical models are given in § 6, based on the observational results of SN 2004dt. We give in § 7 some discussions on the impact of asymmetry on the use of SN Ia as cosmological probes. Finally, in § 8 we provide a brief summary and some

[1] Based on observations collected at the European Southern Observatory (ESO), Chile [ESO program 073.D-0565(A)].

[2] Physics Department, Texas A&M University, College Station, TX 77843.
[3] Lawrence Berkeley National Laboratory, 1 Cyclotron Road, Berkeley, CA 94712.
[4] Purple Mountain Observatory, 2 West Beijing Road, Nanjing 210008, China.
[5] European Southern Observatory, Karl-Schwarzschildstrasse 2, D-85748 Garching, Germany.
[6] Department of Astronomy and McDonald Observatory, University of Texas, Austin, TX 78712.
[7] Astrophysical Science Center, Hiroshima University, 1-3-1 Kagamiyama, Higashi-Hiroshima, Hiroshima 739-8526, Japan.
[8] Department of Astronomy and Astrophysics, University of Chicago, Chicago, IL 60637.
[9] Department of Astronomy, University of Tokyo, Bunkyo-ku, Tokyo 113-0033, Japan.

[10] A very low level of polarization of about 0.1%–0.2% is reported later by Leonard et al. (2005).

general discussions of the most important conclusions we have derived from spectropolarimetry.

2. DISCOVERY AND OBSERVATIONS

2.1. *Discovery*

SN 2004dt in NGC 799 was discovered on an unfiltered image taken on August 11.48 at a magnitude of about 16.1 (Moore & Li 2004). Salvo et al. (2004) reported that a spectrum taken on August 12.72 UT showed SN 2004dt to be a young SN Ia a few days before maximum light. The photospheric expansion velocity deduced from the absorption minimum of Si II 635.5 nm was about 16,500 km s^{-1}, adopting the recession velocity of 5915 km s^{-1} reported by the NASA/IPAC Extragalactic Database (NED) for the host galaxy NGC 799. Patat et al. (2004) reported that a spectrum obtained on August 13.17 UT showed some unusual features. They noted that the O I 777.4 nm transition was particularly pronounced, with a broad symmetric P Cygni profile, and also had an expansion velocity of about 16,800 km s^{-1}. They also report that the Ca II H and K line gave 22,200 km s^{-1} (we think this feature is mostly due to a Si II line; see § 3.2). Patat et al. (2004) suggested that the high velocities of the lines indicated a very early phase. They noted that other intense lines visible in the spectrum were from Fe III and Si III.

2.2. *Observations and Data Reduction*

We observed SN 2004dt with the ESO VLT on 2004 August 13.30 UT with the FORS1 instrument in polarization mode. From preliminary light curves of W. Li et al. (2004, private communication), this corresponds to 6–8 days before optical maximum. Four exposures of 1200 s duration were taken with the wave plate at position angles of 0°, 45°, 22°.5, and 67°.5. Flux and polarization standard stars were observed to calibrate the flux levels and polarization position angles. The data were reduced in a way similar to that described in Wang et al. (2003b).

2.2.1. *Spectrophotometry*

The observations consist of multiple exposures with the air mass varying from 1.02 to about 1.20. The slit size was 1″ and was aligned with the parallactic angle. The seeing was below 1″, which allows for approximate spectrophotometry calibrations. Figure 1 (*top*) shows the total flux spectrum. Starting in the blue, there is no sharp drop of flux blueward of the strong Ca II H and K absorption, as commonly observed in normal SN Ia at optical maximum. The Ca II H and K feature appears very strong, although, as we argue in § 3.2, it should probably be identified as Si II 385.9 nm. The strong line of Si II 635.5 nm shows the typical blueshifted absorption that characterizes SN Ia at 600 nm, but it is especially strong, broad, and fast moving. The minimum corresponds to a velocity of about 17,000 km s^{-1}, and the blue wing extends to about 25,000 km s^{-1}. We also observe a strong line of O I 777.4 nm as pointed out by Patat et al. (2004). This line also showed an absorption minimum at about 17,000 km s^{-1} with the blue wing again extending to about 25,000 km s^{-1}. To first order, the Si and O occupy the same velocity space. Our data show two components of the Ca II IR triplet, a broad absorption at 820 nm and a "notch" indicating a separate, high-velocity component at about 800 nm. These represent velocities of ~16,000 and 23,000 km s^{-1}, respectively. The lower velocity component corresponds approximately to the velocity minimum of Si II and O I. The higher velocity component seems kinematically distinct, as in SN 2001el (Wang et al. 2003b) and SN 2003du (Gerardy et al. 2004), and to correspond roughly to the blue wing of the Si II and O I lines. Despite the likely two-component nature, the highest velocity, again, can be traced to 25,000 km s^{-1} for the Ca II IR triplet, similar to the other high-velocity lines.

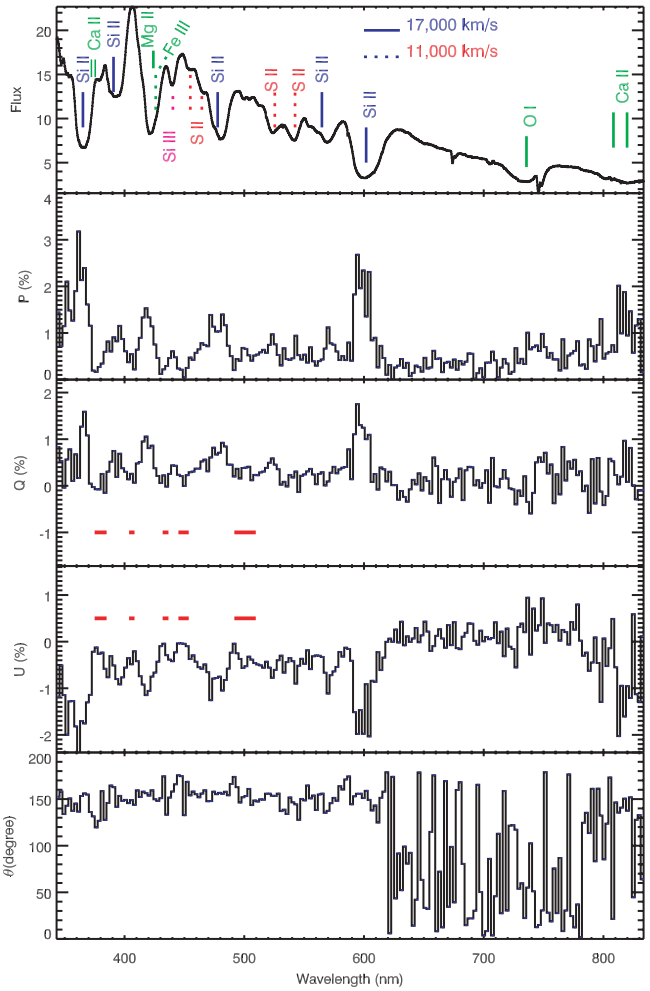

FIG. 1.—Spectroscopy of SN 2004dt deredshifted, assuming a recession velocity of 5915 km s^{-1} of the host galaxy. The five panels give the total flux spectrum, the polarization, P, the reduced Stokes vectors, Q and U, and the polarization angle θ. Typical spectral features are marked on the top panel. The lines are produced by material moving at velocities of 17,000 km s^{-1} (*solid lines*) and 11,000 km s^{-1} (*dotted lines*; see Fig. 3 for a more complete description) in the rest frame of the supernova. Lines from different elements are marked with different colors (*gray scales*). The panels for polarization data are binned to 25 Å. The wavelength regions used to determine interstellar polarization are marked by horizontal lines on the panels for Q and U. Stronger lines tend to be associated with larger degrees of polarization, except for the O I 777.4 nm line.

The strong absorption feature at 421 nm is due to Mg II 448.1 nm, blended with Fe III and Si III lines. If this feature is predominantly Mg II, then the absorption minimum of the Mg II line is blueshifted by 17,000 km s^{-1}, consistent with the lines of Si II, Ca II, and O II. The strength of the 421 nm feature is comparable to the O I 777.4 nm line, as measured by the ratio of line minimum to local continuum.

The absorption minima of the S II "W" lines are measured to be at 523.5 and 543.1 nm, which implies a velocity of only 11,000 km s^{-1}. This is significantly lower than the velocity of the Si II lines. Weak lines at 439.5, 454.2, and 464.0 nm, tentatively identified with Si III 456.0 nm, S II 471.6 nm, and S II 481.6 nm, respectively, also show the much lower velocity of 11,000 km s^{-1}. The presence of Si III 456.0 nm at 11,000 km s^{-1}, not at 17,000 km s^{-1}, shows that doubly ionized Si exists only close to the central region. Silicon is the only element present in two different ionization stages. They share the emerging bimodal distribution of

TABLE 1
SUMMARY OF OBSERVED POLARIZATION FEATURES

Ion	Rest Wavelength(s) (nm)	Radial Velocity (km s^{-1})		Polarization	
		Bulk	Blue Edge	Degree (%)	Angle (deg)
Continuum	350–600	11,000	N/A	0.0	N/A
	600–850	11,000	N/A	−0.3	60
S II	471.6, 481.6, 543.3, 545.9	11,000	15,000	0.3	150
Si III	455.3–456.83–457.5	11,000	...	0.3	150
Ca II	850.03–854.23–866.2	16,000	27,500	0.7–2	150
Mg II	447.1	17,000	28,000	1	150
O I	777.4	17,000	27,500	<0.2	N/A
Si II	385.0, 413.0, 504.1, 505.6 635.5	15,000–17,000	25,000	0.5–2	150

radial velocities: singly ionized silicon has a bulk velocity of 17,000 km s^{-1}, whereas Si III expands with 11,000 km s^{-1}. Table 1 gives a schematic overview of the kinematic properties of the main ions observed.

2.2.2. *Spectropolarimetry*

The second, third, and fourth panels of Figure 1 show the polarization, P, and the reduced Stokes vectors, U and Q. The degree of polarization is corrected for biases due to observational noise using the equations derived in Wang et al. (1997). The Q vector, in particular, shows a total excursion of ~2% with sharp wavelength dependence, indicating strong, intrinsic polarization. The bottom panel of Figure 1 gives the polarization position angle. It is nearly constant from 330 to 630 nm, but then shows a strong change with possibly significant excursions at wavelengths longer than 630 nm. This change could be due to a combination of polarization by interstellar dust and the intrinsic polarization by the supernova ejecta. Note that the polarization position angle is periodic with respect to the position angle on the sky, with a period of 180°.

Figure 2 gives the data in the Q-U plane, where each point represents the Stokes parameters rebinned to 25 Å intervals. The bin size was chosen to be larger than the spectral resolution to minimize correlations among neighboring lines. The total excursion is nearly 3%. The scatter of points is predominantly due to line features. The data points span a range of about 1.5% in Q and more than 2% in U. Figure 2 shows that the bulk of the points fall along the line that represents the "dominant axis" of the geometry (Wang et al. 2001), determined by making a principle component decomposition of the data points on the Q-U plane. The scatter orthogonal to this axis suggests that there are smaller but real deviations in the geometry from this dominant axis that may also constrain the physics of the explosion.

3. THE DISTINGUISHING OBSERVATIONAL FEATURES

3.1. *The Spectral Lines and Profiles*

The colors synthesized from the spectrum give $U - B \sim -0.6$. This blue color (as verified by the strong blue flux in Fig. 1), suggests that this event, if approximately "normal," is close to or before U maximum. This may mean that at this phase, SN 2004dt has not yet been subject to the strong Fe II absorption leading to the characteristic UV deficit of normal SN Ia near maximum light (Wheeler & Harkness 1990; Kirshner et al. 1993).

The strong lines of Si II 635.5 nm and O I 777.4 nm in the total flux spectrum suggest that there is substantial ejected silicon and oxygen, moving at velocities approaching 25,000 km s^{-1}. This is consistent with a significant amount of incompletely burned matter. The lack of a UV deficit suggests that there is not much iron in the photosphere at the phase of these observations. To investigate further the possibility of an iron deficit, we have performed line identifications using the SYNOW code (Fisher et al. 1999). Assuming a composition with only Si II, S II, O I, and Mg II, we found that the observed spectral features are reasonably well explained without requiring iron. What distinguishes SN 2004dt from other Type Ia supernovae appears to be that a larger than usual amount of silicon is required to explain the deep spectral features from Si II. The SYNOW line identification is shown in Figure 3. The absence of Fe features is another striking property of the spectrum of SN 2004dt at this epoch.

The presence of lines at a velocity of 11,000 km s^{-1} suggests that even at this early phase, the ejecta is not Thompson opaque at this lower velocity. The velocity of the Si III 455.3, 456.8, and 457.5 nm blend is only 11,000 km s^{-1}, implying that doubly ionized silicon exists mainly in this lower velocity region. The low-velocity S II line suggests that S is more concentrated in the low-velocity region than Ca, O, Mg, and Si.

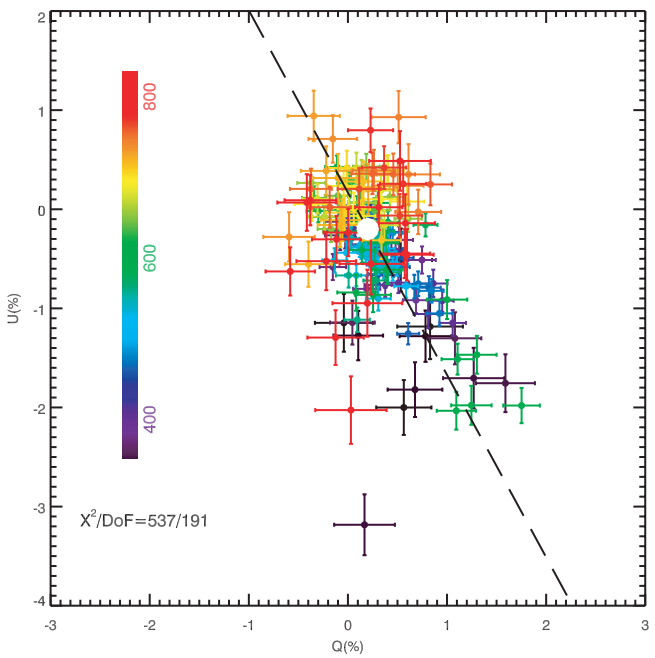

FIG. 2.—Spectropolarimetry of SN 2004dt displayed in the plane of the reduced Stokes vectors Q and U. Note the existence of a dominant axis represented by the solid line. The 1 σ location of the polarization due to interstellar dust is shown as an open circle. The data points are binned to 25 Å.

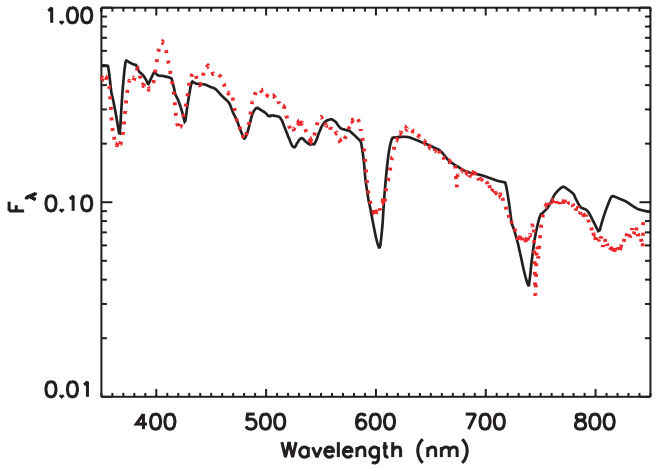

FIG. 3.—Line identifications in the observed spectrum using the SYNOW code. The only ions contributing to the model spectrum (*solid line*) are Si II, Mg II, O I, and S II. Other relevant fit parameters are the following: the ions are distributed in a shell from 16,000 to 25,000 km s^{-1}, with the exception of the S II, which is distributed from 11,000 to 18,000 km s^{-1}; the location of the photosphere is assumed to be at 11,000 km s^{-1}, with the temperature fixed to 11,000 K; the optical depth is assumed to decrease outward with an exponential law with an *e*-folding velocity of 5 km s^{-1}; and the optical depths used in SYNOW are 2.0, 0.5, 0.5, and 1.0 for Si II, Mg II, S II, and O I, respectively. The unusual appearance of the observed Si II profiles is likely due to a combination of the high velocity and overabundance of Si II.

3.2. *The Interstellar Polarization toward SN 2004dt*

From the strong modulation of the raw polarization shown in Figure 1 it is immediately evident that the intrinsic linear polarization of SN 2004dt is exceptionally large. The vectorial nature of polarization can lead to confusing conclusions if the interstellar polarization (ISP) is not properly determined and subtracted; unfortunately, the determination of ISP inevitably requires some model assumptions. We have tried to avoid assumptions that are tied to the models of SN Ia explosions.

The central assumption made here is that the ISP dominates where the continuum polarization of the supernova is the lowest. The effective continuum polarization probably gets decreased by overlapping spectral lines. Since there are many more such lines in the blue portion of the spectrum than in the red portion (Wang et al. 2001, 2003b; Howell et al. 2001), we have selected the regions marked in Figure 1 to represent the minimal intrinsic polarization; they avoid significant discrete absorption features.

It is seen in Figure 2 that the deduced ISP corresponds to $0.2\% \pm 0.1\%$ in Q and $-0.2\% \pm 0.1\%$ in U. This low value is consistent with the absence of an interstellar Na I D line (§ 5.1) if the gas-to-dust ratio of the host galaxy is normal.

In Figure 2 the data points used for the determination of the ISP are embedded in a large cloud of other low-polarization wavelength bins. If, following Wang et al. (2001), a principle-component decomposition technique is used to define the dominant and the orthogonal polarization axes, the ISP will, therefore, be close to the dominant axes. As Wang et al. (2001) have shown, some minor error in the determination of the ISP does not grossly distort a qualitative interpretation if the true ISP is close to the dominant axis.

A similar constellation of data points prevailed in SN 2001el (Wang et al. 2003b). The key corroborating observation was that at later phases the polarization of the continuum as well as of spectral features retreated along the dominant axis and, starting a week after maximum, remained within a similar cloud of low-polarization wavelength bins. A preliminary analysis of later epoch data of SN 2004dt shows a similar behavior. The resulting ISP-corrected decomposition into dominant and orthogonal axis is presented in Figure 4.

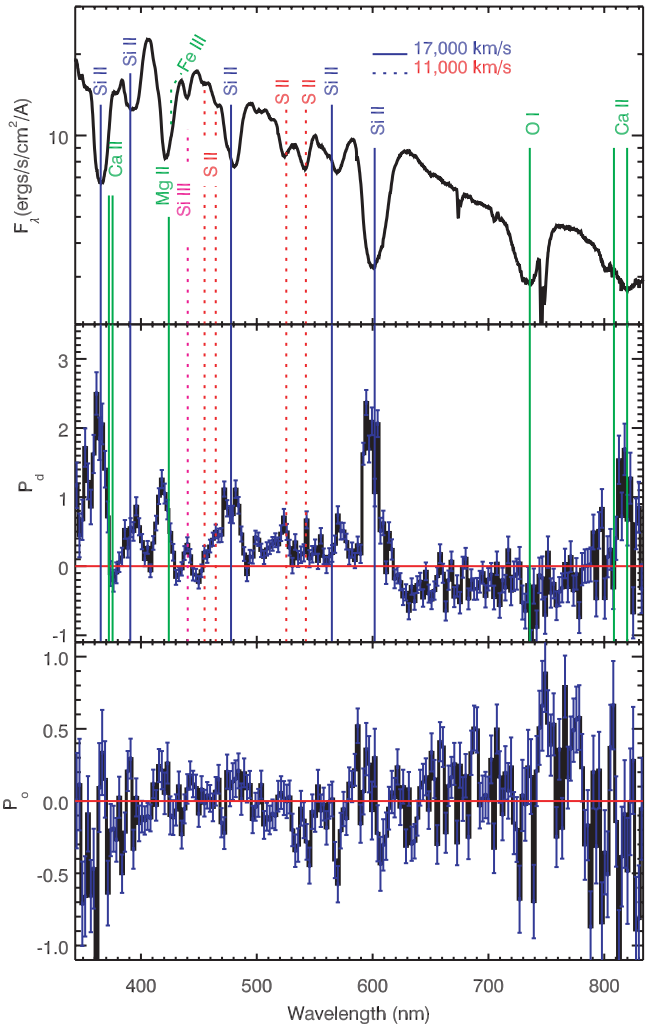

FIG. 4.—The top panel gives the total flux spectra; the next two panels give the polarization spectrum projected onto the dominant axis and the orthogonal axis, respectively. The solid vertical lines mark the positions of the lines of Si II, Mg II, Ca II, and O I, which are typically blueshifted by 17,000 km s^{-1}. The vertical dashed lines mark the positions of the lines of S II, Si III, and Fe III, at a blueshift of 11,000 km s^{-1}. All the polarized features except O I line share the same dominant axis, suggesting that the geometrical structures of Si II, Mg II, and Ca II are the same. No polarization is detected across the O I line. Weaker lines of Si III, and S II show also polarization along the dominant axis. The data are binned to 25 Å. Note that the polarization features at 747.0 nm may not be reliable because of telluric absorption.

3.3. *The Intrinsic Polarization of SN 2004dt*

Ultimately, the choice of interstellar polarization must depend on the totality of observations and a self-consistent picture of the physics of the explosion and radiative transfer through the complex ejecta. Important details of the interpretation of the data may yet depend on the particular placement of the ISP. For this paper we have attempted to restrict our discussion to features that are relatively independent of the choice of the ISP.

SN 2004dt shows a polarization spectrum unlike any SN Ia yet observed. Compared to the well-observed SN 2001el, the Si II lines are especially prominent in the polarization spectrum, but the lines of the Ca IR triplet are less so.

With the above choice of the interstellar polarization, we see from Figure 4 that the absorption minima of the P Cygni profiles

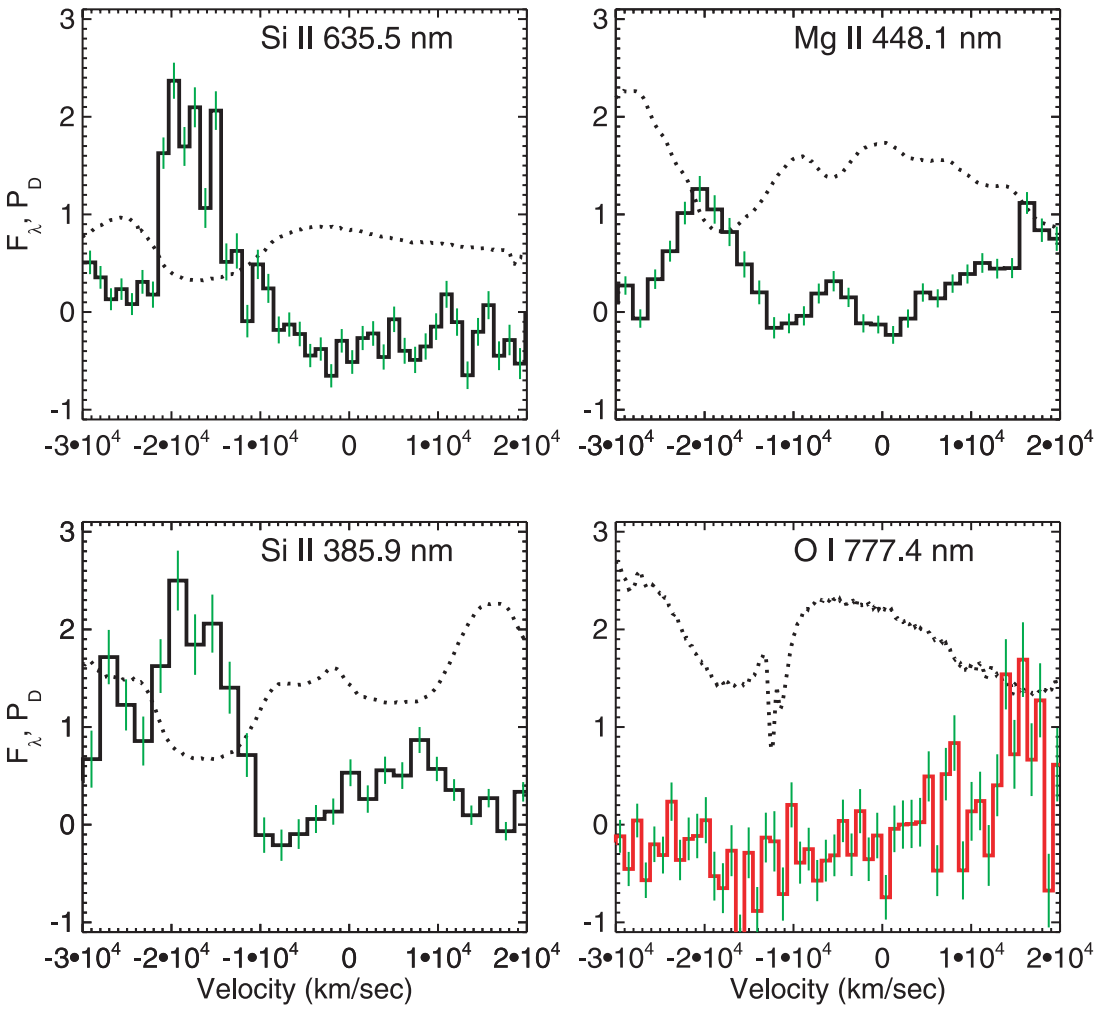

FIG. 5.—Absorption features in the total flux spectrum and the polarization profiles along the dominant axis shown as a function of velocity for the lines of Si II 635.5 nm (*top left*), Mg II 447.1 nm (*top right*), O I 777.4 nm (*bottom right*), and Si II 385.9 nm (*bottom left*). The dotted lines show the P Cygni profiles. The solid histograms shows the spectropolarimetry profiles. Note that the polarization is detected in all lines except that of O I. Note also that the emission component of the P Cygni profiles are all blueshifted by about 4000 km s^{-1}.

correspond in general to the peaks of the spectropolarization profiles. Along the dominant axis polarization spectrum, the polarization in the range 620–720 nm is around −0.3% for the choice of interstellar polarization adopted in Figure 4. This wavelength range shows no strong spectral lines, and it is likely that continuum polarization by Thompson scattering dominates this wavelength region.

The high-quality data we obtained allow for a detailed comparison of the spectral and spectropolarimetry profiles of several distinct lines, as shown in Figure 5. Spectropolarimetry allows us to revisit the issue of line identification as discussed already in § 3.1.

3.3.1. Si II *Lines*

One of the strongest polarization features in Figures 4 and 5 is the spike at 600 nm, which corresponds to the Si II 635.5 nm line. The strength of this feature, ∼2%, is unprecedented in the observed polarization spectra of SN Ia. There is also a strong spike in the polarization at 365.0 nm, the location of the Ca H and K line. We suspect this is due primarily to Si II 385.0 nm, which is only slightly contaminated by the Ca lines. Note that the amplitude of this polarization feature, ∼2%, is nearly identical to that of the Si II 635.5 nm line. No other features in the polarization spectrum show this level of polarization. The spectral and spectropolarimetry profiles of the Si II 385.9, 635.5 nm lines are shown in Figures 5*a* and 6*c*, respectively. The polarizations are the highest at the absorption minima of these two features. The spectral and spectropolarization profiles of the two lines are remarkably similar. The peaks of polarization occur at a blueshift of about 20,000 km s^{-1} for both lines, then drop sharply at higher velocity. This strengthens our identification that they are from the same ionic species. The dominant-axis spectrum shows another feature at 390 nm, which we attribute to Si II 413.0 nm. Note, however, that the same feature was tentatively identified as C II 426.7 nm, with an expansion velocity of about 24,100 km s^{-1}, by Patat et al. (2004). Our identification with Si II would put the line at the same velocity, of about 17,000 km s^{-1}, as the other Si II lines.

The line at 480 nm can be due to the blend of Si II 504.1, 505.6 nm and Fe II 491.3, 501.8, 516.9 nm. As can be seen in Figure 4, the contributions from Fe II must be small, as evidenced by the absence of the strongest Fe II line in this wavelength region, Fe II 516.9 nm, in the total flux spectrum. The small feature at 570 nm is likely to be due to Si II 595.8, 597.9 nm. To the red of the Si II 635.5 nm line, the polarization dips and is then constant to about 720 nm. With these identifications, all the Si II lines have velocities from 15,000 to 17,000 km s^{-1}.

The lines of Si II 413 nm, Mg II 447.1 nm, and Si II 504.1, 505.6 nm all have polarization ~1% in Figure 4, significantly less than the strongest polarized lines of Si II, but suggesting some commonality in their geometry. All these lines have similar dominant polarization position angles.

3.3.2. Si III *and* S II *Lines*

Weaker lines from Si III and S II are also polarized, at a level of about 0.3%, and have polarization position angles similar to those of the Si II lines. The blueshifts of the absorption minima for these lines are around 11,000 km s^{-1}, which is significantly lower than the strong Si II lines.

3.3.3. Mg II 420.0 nm

The polarization feature at 420 nm is mostly due to Mg II 447.1 nm. The profiles are shown in Figure 5*b* for this line. Like the polarizations of the Si II 635.5 nm and Si II 385.9 nm lines, the polarization of the Mg II 447.1 nm line peaks also at a blueshift of around 20,000 km s^{-1}, but the polarization does not exhibit a sharp drop at higher velocities and appears to extend to even higher velocities than those of the Si II lines.

3.3.4. Ca II *Lines*

The polarized spectral feature at 820 nm is clearly due to the Ca II IR triplet; the absorption minimum of the Ca II feature shows a velocity of 16,000 km s^{-1}, consistent with that of the Si II lines. Note that, unlike SN 2001el, which showed a highly polarizing detached Ca II shell at a velocity of 22,000 km s^{-1}, the high-velocity component of the Ca II IR triplet of SN 2004dt with a similar velocity is not particularly strong, nor does it have an especially high polarization. SN 2001el and SN 2004dt are distinctly different in this regard. The lower velocity component of the Ca II IR triplet in SN 2004dt shows a polarization spike of about 0.7%–2%, comparable to the Mg II line. The higher velocity component shows a spike of about 0.3%, comparable to the S II and Si III lines. These polarized components of Ca II seem to share approximately the same polarization angle as all the other polarized lines, ~150°.

At the same velocity as the Ca II IR triplet, only a weak dip is observed for the Ca II H and K lines. The weak Ca II H and K lines do not produce a prominent polarized feature.

3.3.5. O I 777.4 nm *Line*

Despite the very strong spectral line of O I 777.4 nm in the total flux spectrum, there is little sign of that feature in the polarization spectrum. The spectral and spectropolarimetry profiles of this line are shown in Figure 5*c*. This low polarization is in sharp contrasts to all the other strong lines from Mg II, Si II, and Ca II.

3.4. *Summary of Observed Features*

The rather diverse spectral information extracted from our data can be summarized as follows (see also Table 1): (1) lines of Mg II, O I, Ca II, and Si II are at the highest velocities, their absorption minima are typically blueshifted by 17,000 km s^{-1}, and the lines can be traced to a velocity of around 25,000–28,000 km s^{-1}; (2) the S II lines have absorption minima at only 11,000 km s^{-1}; the highest velocity of these features is less than 15,000 km s^{-1}; (3) the absorption minimum of the Si III 455.3, 456.8, and 457.5 blend is blueshifted by 11,000 km s^{-1}; (4) all the high-velocity features except that from O I 777.4 nm are significantly polarized, at levels from 0.7% to 2.2%, with two features of Si II being especially distinct; (5) weak lines from S II and Si III are also polarized, at a level of about 0.3%, but share the same polarization position angles as those of the other polarized lines; (6) the high-velocity shell of Ca II has a velocity comparable to the blue wings of the strong lines, but with a polarization amplitude and angle comparable to S II and Si III.

4. THE INFERRED EJECTA GEOMETRY

4.1. *Bubbles and Plumes*

A critical issue is whether the observed polarization indicates a clumpy ejecta or a globally aspherical structure with little in the way of small-scale features. The *Q-U* diagram provides a powerful tool to study the clumpiness of the ejecta. If the asymmetry is caused by an axially symmetric structure, the resulting polarization will inscribe a straight line on the *Q-U* diagram. This is easy to understand, as the polarization position angle is only related to the position angle of the symmetry axis on the sky. Deviations from the straight line on the *Q-U* diagram are expected only if the structure departs from axial symmetry, for instance by being fragmented and clumpy.

The observed polarization for each line can be fit by a linear relation:

$$U = \alpha + \beta Q. \quad (1)$$

Such a fit gives the dominant axis of that particular line in the *Q-U* plane. The goodness of this fit is a direct measure of the smoothness of the ejecta. For the strongest lines, the region for this linear fit was chosen to be from −25,000 to −10,000 km s^{-1} for Si II 635.5, 385.9 nm and Mg II 448.1 nm; this corresponds closely to the absorption minima of the P Cygni profiles. The corresponding range was chosen to be from −25,000 to −13,000 km s^{-1} for the O I 777.4 nm line to avoid contamination by telluric features. The situation is less clear for weaker lines, which are often blended with other lines. For the S II W feature, the velocity range was taken to be from −15,500 to −9,500 km s^{-1}, and both lines were used for the linear fit. For Ca II IR triplet, the lines are blended and the range of the fit was taken to be 786.0 to 834.2 nm.

Figure 6 shows the *Q-U* diagrams for the strongest lines, Si II 385.9 nm and 635.5 nm, Mg II 448.1 nm, and O I 777.4 nm. Table 2 gives the details of the linear fits for all the lines that allow for a linear fit on the *Q-U* plane. The columns in Table 2 are as follows: the atomic line, the blueshift range of the data used in the fit, α, β, the resulting position angle of the straight line, the χ^2, the degrees of freedom of the fit, and the probability that the association with a straight line is by chance.

The linear fit provides a good description to the observed *Q-U* diagram only for the Mg II and the S II lines. For the other ionic lines, the fits are highly inconsistent with a straight line. It is interesting to note that the O I line, despite its lack of a well-defined axis, is inconsistent with a random Gaussian distribution, and therefore the data actually suggest intrinsic polarization of the oxygen, but with no well-defined symmetry axis. The Si II and Ca II lines all show clear evidence of a dominant axis, but with significant intrinsic deviations from the dominant axis. Only the Mg II gives a good fit (χ^2 per degree of freedom ~1) indicating a distribution along a single, well-defined axis with no measurable deviation due to fragmentation or clumping. The Si II 635.5 nm line gives a fit with χ^2 per degree of freedom 4, and a position angle that only differs from that of Mg II by about 2 σ. This suggests that the silicon may share the same dominant axis as the magnesium, but with significant clumping.

This analysis suggests that the distribution of silicon follows some large-scale asymmetry, which gives rise to the dominant

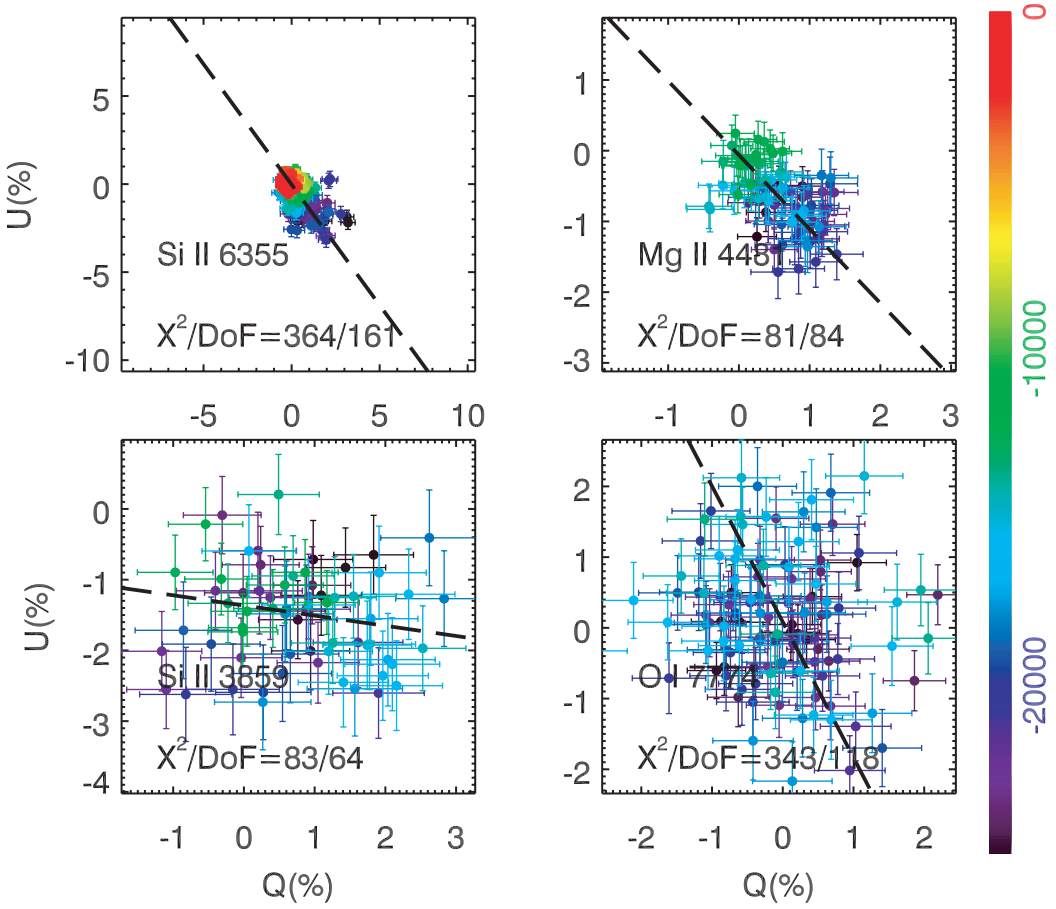

FIG. 6.—*Q-U* diagrams of the strongest lines and the corresponding linear fits. The dashed lines are the results of the linear fits. The ranges of the data points used for the fits are given in Table 2 and are from −25,000 to −10,000 km s^{-1} for these lines. The panels are for the lines of Si II 635.5 nm (*top left*), Mg II 448.1 nm (*top right*), O I 777.4 nm (*bottom right*), and Si II 385.9 nm (*bottom left*). Only the Mg II line is consistent with a straight line, indicating a simple axially symmetric geometry with no detectable clumping (see text).

axis, but that there are also prominent smaller scale structures in silicon that lead to significant deviations from the dominant axis in the *Q-U* diagrams. The polarization of the Si III line at lower velocity, but with the same position angle, suggests that this asymmetric silicon structure extends from at least the photosphere at about 11,000 km s^{-1} all the way to the highest observable velocity for the Si II lines, i. e., 25,000 km s^{-1}. The transverse scale of this silicon-rich structure should be comparable to the size of the ejecta where the Thompson optical depth is around 1, so that the asymmetric line opacity of the structure will have a large enough area covering factor to produce both the strong absorption and the large degree of polarization. This radially extended silicon structure is fragmented or clumpy. The size of the small-scale structures that give rise to the departure from the

TABLE 2
PROPERTIES OF POLARIZED LINES

Line	V_{range} (km s^{-1})	α	β	P.A.[b] (deg)	χ^2	DOF	Probability
Si II 635.5	(−25,000, −10,000)	−0.03 ± 0.05	−1.37 ± 0.09	$153.1^{+0.97}_{-0.11}$	364	161	$<10^{-6}$
Si II 385.9	(−25,000, −10,000)	−1.36 ± 0.11	−0.14 ± 0.11	$175.9^{+3.2}_{-3.1}$	90	68	0.047
Mg II 448.1	(−25,000, −10,000)	−0.06 ± 0.10	−1.04 ± 0.16	$156.8^{+2.3}_{-2.0}$	81	84	0.54
O I 777.4	(−25,000, −13,000)	0.08 ± 0.13	−1.92 ± 0.55	$148.8^{+4.3}_{-2.8}$	348	118	$<10^{-6}$
Si III 456.5	(−15,000, −5,000)	−0.16 ± 0.05	−0.24 ± 0.17	$173.2^{+4.8}_{-4.3}$	101	56	0.05
S II 562.3,544.8	(−15,000, −9,500)	−0.18 ± 0.15	−1.19 ± 0.41	$155.0^{+6.0}_{-3.0}$	191	83	$<10^{-6}$
Ca II IR triplet	(−24,000, −7,000)[a]	−0.81 ± 0.13	2.39 ± 0.68	$33.7^{+2.3}_{-3.8}$	486	187	$<10^{-6}$
Continuum	(640, 700)[c]	0.14 ± 0.03	−0.14 ± 0.13	$175.9^{+3.7}_{-3.8}$	465	234	$<10^{-6}$

[a] Velocity calculated with respect to the rest frame wavelength of 854.2 nm.
[b] The errors on P. A. are highly non-Gaussian when the slopes of the linear fits are not well constrained. The P.A. is periodic, with period of 90°. The angle is practically undetermined for Si II 385.9 nm, O I 777.4 nm, and the Ca II IR triplet.
[c] Wavelength range in nanometers.

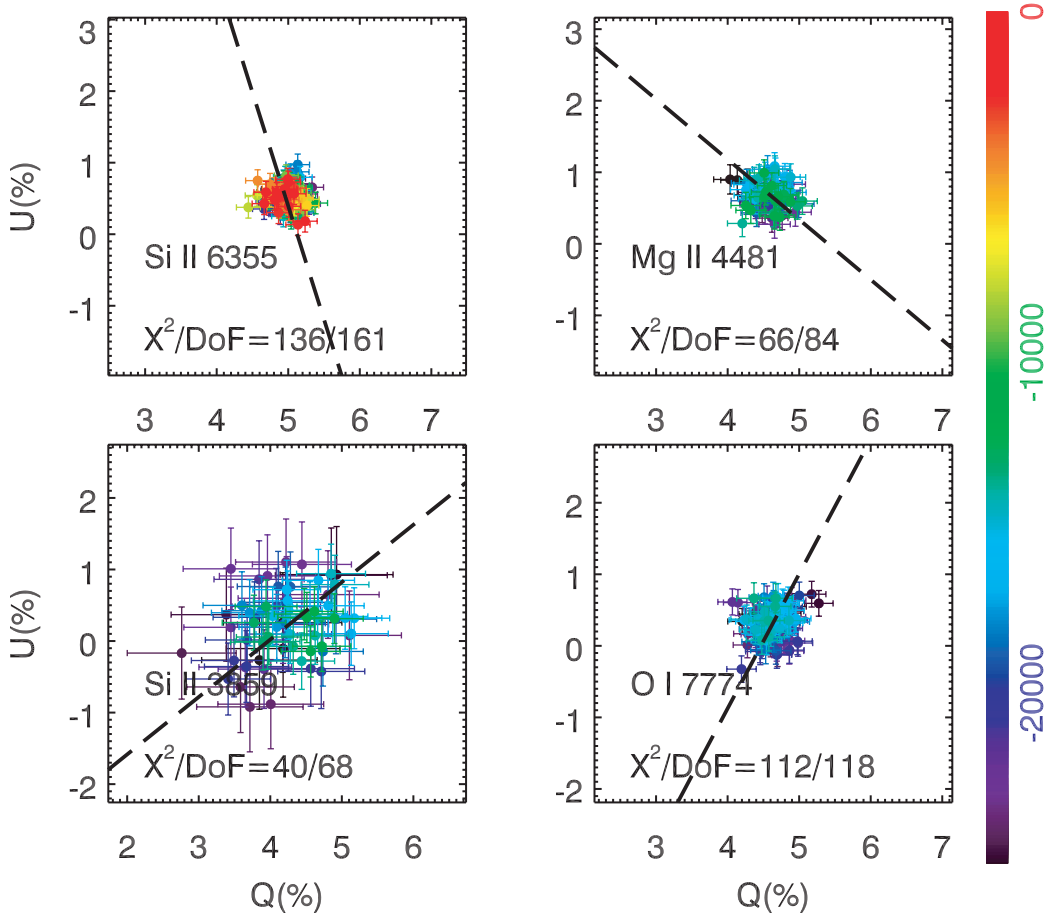

FIG. 7.—*Q-U* diagrams of the polarized standard star HD 316132, at wavelength regions identical to the corresponding panels in Fig. 6. The dashed lines are the results of the linear fits. The ranges of the data points used for the fits are given in Table 2 and are from −25,000 to −10,000 km s^{-1} for these lines. The panels are for the wavelength regions corresponding to those of Si II 635.5 nm (*top left*), Mg II 448.1 nm (*top right*), O I 777.4 nm (*bottom right*), and Si II 385.9 nm (*bottom left*).

dominant axis must be larger than 1200 km s^{-1}, which corresponds to the approximate resolution of the data and to the bin size of the data points on the *Q-U* diagrams given in Figure 6. Our data are not sensitive to clumps smaller than 1200 km s^{-1}.

The fact that the Mg II line is *consistent* with a straight-line fit in the *Q-U* plane with no significant deviation from the principal axis means that, although its geometry follows quite nearly that of the Si II globally, the magnesium has a smooth large structure with no noticeable small-scale clumps or fragments. This has several implications. First, the success of the straight-line fit for this line implies that the errors associated with the *Q* and *U* vectors are reasonable; this lends confidence in the robustness of the fits for the other lines. Second, this implies that the distribution of magnesium is less clumpy than that of silicon. This could be understood if some amount of magnesium coexists with the silicon-rich clumps but that there are magnesium-rich regions that do not contain noticeable amount of silicon. The number density contrast of magnesium in different clumpy regions (presumably generated by explosive carbon burning) must be small; the number density contrast of silicon in those different clumpy regions must be large.

The lack of a clear dominant axis for the O I line and the obvious inconsistency of the data with random Gaussian distribution on the *Q-U* plane suggest that the distribution of oxygen is even more pervasive than magnesium, but the opacity must be very clumpy, perhaps due to large variations of oxygen abundances in different chemical regions.

We have extensively tested our error models of the data points of the *Q-U* vectors and found that the dominant errors are due to photo statistics, not due to unknown systematic errors. This is done by analyzing observations of polarized and unpolarized standard taken in each observing campaign. As an example, we show in Figure 7 the *Q-U* diagrams of a polarized standard star HD 316132, taken on 2004 August 8, with exposure time of 12 s at each wave plate position angle. This polarized standard star is polarized at 4.57% ± 0.02% in *B* band, at a position angle of 4°.3 ± 0°.2. The same wavelength region identical to those of the corresponding spectral lines for SN 2004dt were plotted in Figure 7, but now the data points were taken from the observed spectropolarimetry data of HD 316132. In these regions, the data are can all be very well fitted by a straight line, with the χ^2 per degree of freedom all below 1.

The *Q-U* diagram of SN 2004dt shows undoubtedly that at the highest velocity, the ejecta of SN 2004dt are highly asymmetric and turbulent.

4.2. *Nucleosynthesis at the Highest Velocities*

The null detection of polarization across the O I 777.4 nm line demands further explanation. From the spectral profile, we know that oxygen coexists with silicon, magnesium, and calcium. Why

does the O I 777.4 nm line not share the same polarization properties of lines from the other elements?

A simple explanation is that oxygen is distributed in a different way from silicon, magnesium, and calcium, although they share the same velocity space. Oxygen is likely more pervasive in the outer region, but the protrusions of products from nuclear burning are distributed in holes or filaments in this region. Such protrusions also contain oxygen. In such a geometry, the polarization from oxygen and from the other elements is drastically different, as their geometrical structures are not identical but occupy different regions.

If so, then the null detection of polarization across the O I 777.4 nm line implies that the oxygen-rich region does not exhibit the same asymmetric geometry as the magnesium-silicon-rich regions. This would require that the magnesium/silicon-rich regions also contain a significant amount of oxygen, so that oxygen appears to be more "spherically" distributed. Indeed, in explosive carbon burning, oxygen is expected to coexist with magnesium, a principal burning product.

The observed high degree of polarization of high-velocity magnesium suggests that the magnesium-rich structure was created by explosive carbon burning. The fact that the magnesium structure is polarized with about the same amplitude and position angle as the silicon lines also shows that magnesium is not confined to magnesium-rich, silicon-poor regions, but also exists in silicon-rich regions. This in turn suggests that the oxygen that must be present outside the magnesium/silicon structure in order to have a very small net polarization must be the preexplosion oxygen from the progenitor white dwarf.

The unusual polarization of SN 2004dt is closely related to the observed velocity structures of the various ions. In the outermost portions, preexplosion oxygen coexists with newly synthesized Si, Mg, and Ca. This outermost layer moves at a velocity around 17,000 km s^{-1} and the highest velocity approaches 25,000 km s^{-1}. The silicon-rich layer extends deep inward to a velocity of around 11,000 km s^{-1}, as evidenced by the presence of Si III and S II lines at that velocity. The broadness and unusually high blueshift of the Si II lines are evidence that these lines are optically thick. Iron and sulfur are noticeably absent in the high-velocity layer. The strong polarization observed across the P Cygni lines of the newly synthesized elements is the result of the asymmetric distribution of the chemical elements in this layer. The polarization position angles of these lines are similar, suggesting that they share a common geometrical structure, but with oxygen permeating the whole structure, magnesium occupying a globally asymmetric region, and silicon occupying a similar globally asymmetric region, but which is, in addition, being broken into clumps or fragments.

The structure of the ejecta is sufficiently asymmetric that spectral lines can be formed in significantly different velocity regions. The attribution of the polarization to asymmetric chemical distributions requires the structures to have considerable radial extent because the angle of the dominant axis is the same for lines formed at different depths, that is, for both Si II at 17,000 km s^{-1} and Si III at 11,000 km s^{-1}. The photosphere in the conventional sense of Thompson optical thickness probably has a complicated geometry that will complicate attempts to understand the radiative processes. For simplicity, one may still assume a photosphere that is located at a velocity much smaller than the 17,000 km s^{-1}, as derived from the absorption minima of the P Cygni lines of Si II lines. The weaker S II W lines and Si III lines at 439.5, 454.0, and 464.0 nm may provide a hint of the location of the photosphere. If so, at least along certain lines of sight the photosphere is at a velocity as low as 11,000 km s^{-1}. This rather low photospheric velocity may not be as surprising. From light-curve fitting, we know that the premaximum luminosity of SN Ia rises approximately as t^2 (Goldhaber et al. 2001), which implies a photosphere at a fixed velocity if the atmosphere is approximated by a blackbody. A photospheric velocity of 11,000 km s^{-1} agrees with the observed luminosity and light-curve behavior of typical SN Ia.

4.3. *Continuum Polarization and the Geometry of the Photosphere*

We note that most of the discussion in this paper relies on polarization variations across spectral features, not on the level of continuum polarization. We do not elaborate on the geometrical structure of the photosphere. With the complicated geometry shown by the various lines, the continuum may be formed in a complicated clumpy environment. It is likely not to have a smooth geometry like the one assumed for ellipsoidal models. The fact that the emission peaks of the strongest P Cygni profiles are all blueshifted by about 4000 km s^{-1} (see Fig. 5) suggests that there is a substantial amount of electron scattering at high velocities. The rather extended region of electron scattering effectively blocks the receding side of the ejecta and can shift the emission peak of the P Cygni profile to the blue. This interpretation of the strong blueshift has to be reconciled with the presence of faint spectral line features at velocities as low as 11,000 km s^{-1} through more detailed line profile modeling. Lacking such models, it should be remarked, however, that a clumpy ejecta is able to produce P Cygni profiles with a blueshifted emission peak together with absorption features at low velocity (Wang & Hu 1994). In such a scenario the patchy opacity structure allows formation of spectral features at low velocity together with shielding of the receding side of the supernova atmosphere.

Taking the adopted components of interstellar polarization at face value, we can see that the level of continuum polarization can be as low as 0.2%–0.3%, consistent with what was found for SN 2001el. The amplitude of continuum polarization is larger in the red part of the spectrum than in the blue part, but with the sign of the polarization flipped. The relatively low level of continuum polarization does suggest that the asphericity of the photosphere is not very large, perhaps only at a level of less than 10%, as has been derived for other Type Ia supernovae, such as SN 1996X (Wang et al. 1997) and SN 2001el (Wang et al. 2003b). The exact level of continuum polarization awaits a full analysis of the data set, which covers postmaximum phases of the supernovae.

5. SN 2004dt AS A MEMBER OF A SUBCLASS OF SN Ia

5.1. *Spectroscopically Similar Events*

SN 1997bp and SN 2002bo displayed high-velocity absorption features similar to those of SN 2004dt. Strong polarized features were also observed across the Si II 635.5 nm line for both SN 1997bp and SN 2002bo. Discussion of the polarization features of SN 1997bp and SN 2002bo will be given in a forthcoming paper. We discuss here only their distinct spectroscopic behavior. As pointed in Benetti et al. (2004), supernovae such as SN 1984A (e.g., Branch 1987) and SN 2002bo show unusually high velocity lines. A comparison of the spectra of SN 1997bp, SN 2002bo, SN 2004dt, and some spectroscopically normal SN Ia is shown in Figure 8. The characteristic behavior of SN 1997bp, SN 2002bo, and SN 2004dt is that they appear spectroscopically normal, but with the lines much broader and at much higher velocities. Benetti et al. (2004) suggest that for this group of supernovae the burning to silicon penetrated to higher layers than in

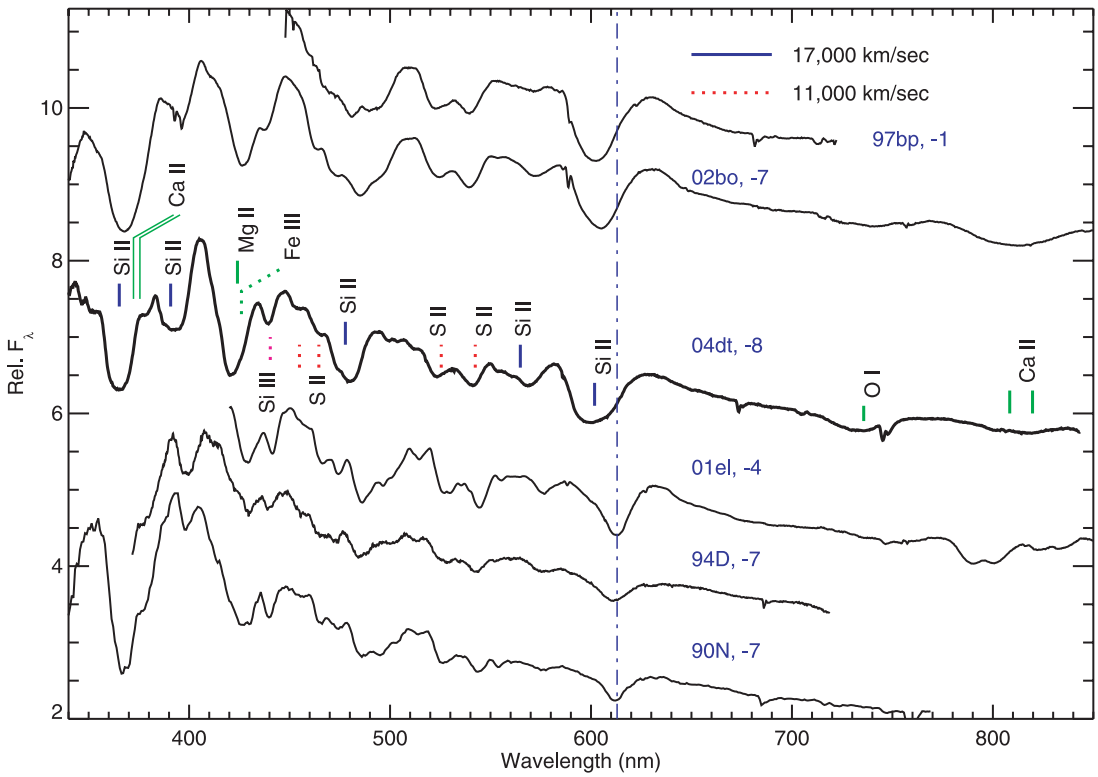

FIG. 8.—Comparisons of spectra of SN 1997bp, SN 2002bo, SN 2004dt, SN 1990N, SN 1994D, and SN 2001el before optical maximum. The data of SN 1997bp were obtained at the 2.1 m telescope at McDonald Observatory through our program of supernova polarimetry (Wang & Wheeler 1997). The data on SN 2002bo and SN 2001el were obtained by our supernova polarimetry program at the VLT (Wang et al. 2003b). The data of SN 1994D are from Patat et al. (1996). The data of SN 1990N are from Jeffery et al. (1992). The Si II 635.5 nm lines of SN 1997bp, SN 2002bo, and SN 2004dt are significantly broader than those of SN 1990N, SN 1994D, and SN 2001el around optical maximum. The vertical line marks the absorption minimum of the Si II 635.5nm line of SN 2001el, SN 1994D, and SN 1990N. The Si II 635.5nm lines of SN 1997bp, SN 2002bo, and SN 2004dt show significantly larger blueshift than those of SN 2001el, SN 1994D, and SN 1990N.

more normal SN Ia. The high-velocity, broad lines can be understood by the presence of a fast-moving shell that is rich in intermediate-mass elements and preexplosion oxygen. The extension of this shell in velocity space requires detailed spectral modeling.

Both SN 1997bp and SN 2002bo show strong narrow Na I D absorption, which implies that they suffer considerable amount of dust extinction from the host galaxy. The equivalent widths of the Na I D absorption are 1.5 and 2.5 Å for SN 1997bp and SN 2002bo, respectively. No strong Na I D line is detected for SN 2004dt. For SN 1984A, Barbon et al. (1989) derived $E(B-V) = 0.45 \pm 0.05$. Kimeridze & Tsvetkov (1986) found $A_B = 1.2 \pm 0.2$. Although these values are uncertain, the observed color around maximum does suggest large interstellar extinction. For SN 1997bp, Riess et al. (1998) give $A_V = 0.62$, suggesting $E(B-V) \approx 0.2$. A significant amount of dust along the light of sight of SN 1997bp in the host galaxy is also consistent with the presence of a strong Na I D line. Benetti et al. (2004) found $E(B-V) = 0.43 \pm 0.10$ for SN 2002bo, in agreement with the observed strong Na I D in SN 2002bo. SN 2004dt does not show a noticeable Na I D line, and final light curves are not yet available to estimate the dust content on the line of sight; however, our flux-calibrated spectrum shows $B-V \approx 0.07$ at around day -7. Although uncertain, this implies an $E(B-V)$ of 0.14–0.2 when compared to colors of typical SN Ia at comparable epoch. Typical $B-V$ for an unextinguished supernova at this phase is around -0.07 (e.g., Phillips et al. 1999). These values of $E(B-V)$ are significantly larger than typical values of $E(B-V)$ found for Type Ia supernovae (Knop et al. 2003).

It is not clear to us whether the extinction of these supernovae is caused by circumstellar or interstellar dust. High-resolution spectroscopy may be helpful in this regard, but it may be difficult to use high-resolution spectroscopy alone to tell whether the dust is within a few parsecs or a few hundred parsecs from the progenitor. Late-time light echo observations (Patat 2005; Wang 2005) combined with late-time polarimetry may set more direct constraints on the location of the absorbing dust. A larger sample of SN 2004dt-like objects will resolve the issue of how strongly they are associated with dusty environments.

All of the four Type Ia supernovae identified to have abnormally high velocity Si II lines show also evidence of unusually large reddening by the dust in the host galaxy. Both SN 1997bp and SN 2002bo are found to be significantly polarized, at levels around 1%–2%. There were no polarimetry data on SN 1984A. This group of objects is likely to be characterized by high velocity, high dust extinction, and intrinsically large polarization before optical maximum.

We do not yet know whether these high-velocity Type Ia supernovae form a separate subgroup of SNe Ia, or whether they are simply a familiar subgroup of objects viewed at a special angle. For the latter possibility, SN 1991T-like events may be candidates to be the counterparts viewed at different angles. The only other subgroup of SNe Ia known to be associated with dusty environments is SN 1991T-like events. Perhaps SN 1991T-like objects are viewed in a direction with very little intermediate-mass elements in the outer layers, whereas SN 2004dt-like objects are the same objects viewed in the direction with substantial preexplosion elements on the outside.

5.2. *SN 20024dt and Other Polarized Supernovae*

SN 2004dt continues to add to the data base that strongly suggests that SN Ia are polarized in a very interesting fashion, but with a variation from event to event that we are just beginning to probe. The observations have revealed both high- and low-velocity spectral features about a week before optical maximum. Strong variation of polarization across spectral lines of intermediate-mass elements, especially silicon, is observed; but most puzzling is nondetection of polarization in the O I 777.4 nm line.

SN 2004dt is different than SN 2001el. For the latter event, the strongest polarization feature was the high-velocity component of the Ca II IR triplet, with Si II polarized at a much lower level than the Ca II IR triplet. For SN 2004dt, the polarization of the Ca II IR features is prominent, but the polarization levels of the lines of Si II are the strongest. SN 2001el showed continuum polarization at the level of about 0.3%. SN 1996X tentatively showed similar levels of continuum polarization. As we discussed before, the precise level of continuum polarization of SN 2004dt is difficult to determine because of the highly polarized spectral features. With the adopted level of interstellar polarization, the continuum level may be comparable to that of SN 2001el and SN 1996X; however, the large polarization across most of the spectral lines makes SN 2004dt distinctively different from SN 2001el. In Wang et al. (2003b), we speculated that it is important to study the correlations among the degree of polarization of the high-velocity Ca II IR triplet, the strength of the high-velocity component of the Ca II IR triplet, and the velocity of the Ca II IR triplet. The observations of SN 2004dt appear to be inconsistent with this speculation, as the polarization of SN 2004dt is slightly higher in the Ca II IR triplet than in SN 2001el, despite the fact that SN 2004dt shows a weaker high-velocity Ca II IR triplet. The observations also seem to confirm, however, the speculation that supernova with overall higher velocity should show larger polarization. Obviously, more spectral polarization data are needed.

6. COMMENTS ON THEORETICAL MODELS OF TYPE Ia SUPERNOVA EXPLOSIONS

SN Ia involve the combustion of a degenerate C-O white dwarf of the Chandrasekhar mass in a binary system (Whelan & Iben 1973; Nomoto 1982a, 1982b). Major theoretical questions concern the ignition and propagation of the flame through the white dwarf. Three major scenarios have been proposed: detonation (Arnett 1969; Hansen & Wheeler 1969), deflagration (Nomoto et al. 1976, 1984), and delayed detonations (Khokhlov 1991; Yamaoka et al. 1992; Woosley & Weaver 1994). Three-dimensional (3D) calculations show that pure deflagration models leave unburned carbon and oxygen mixed into the center (Gamezo et al. 2003; Reinecke et al., 2002). Delayed-detonation models leave very little unburned carbon and tend to produce the observed stratified composition structure (Gamezo et al. 2004; Marion et al. 2003; Höflich et al. 2002, 1995; Wheeler et al. 1998).

6.1. *Deflagration*

In SN 2004dt, we see a highly asymmetric and clumpy structure in silicon that extends from at least as deep as 11,000 km s^{-1} to at least 17,000 km s^{-1}. This fragmented structure could, in principle, be consistent with the turbulent structure produced in 3D simulations of deflagration models (Gamezo et al. 2003; Röpke et al. 2003). The layer at velocity around 17,000 km s^{-1} shows preexplosion oxygen and fragments of intermediate-mass elements, but with no iron. Deeper inside, sulfur is found at a velocity around 11,000 km s^{-1}, which shares the same asymmetry signature as the high-velocity, oxygen-rich layer.

In deflagration models silicon coexists with iron; the absence of strong iron features in the spectrum may be inconsistent with published pure deflagration models, but we caution that the exact amount of iron that can be hidden in the spectra without producing pronounced spectral features is uncertain, and quantitative spectral modeling is needed to set the constraints on deflagration models. The velocities of the silicon and magnesium are significantly higher than predicted by pure deflagration models. It thus seems that turbulent deflagration models are capable of producing the observed clumpy composition structure but are perhaps incapable of producing the kinematics of the ejecta. Deflagration models also predict unburned matter, C and O, mixed down to low velocities. Subsequent observations of this event will help to put constraints on this possibility. Deflagration models also tend to leave a layer of completely unburned C and O on the outside. It is very important to put limits on the amount of carbon in the spectra.

6.2. *Delayed Detonation*

An alternative is the delayed detonation (DD) model (Khokhlov 1991). This model assumes that at a certain stage of deflagration the nuclear burning becomes supersonic and therefore switches to a detonation. In order to have a high-velocity partially burned layer, there must be significant preexpansion (due to the subsonic deflagration stage) before the onset of detonation, which sufficiently reduces the density of the progenitor white dwarf before the nuclear-burning flame propagates to the surface layers. It may also be possible that there is a layer on the surface of the progenitor white dwarf with a density that is too low to burn at all. Because of the low density near the surface, the products of the nuclear reactions are mostly intermediate-mass elements. A strong detonation wave is unlikely to generate a turbulent silicon layer such as we apparently observe in SN 2004dt. One possible way out is that the detonation wave weakens significantly near the surface of the star, in which case the cellular structure associated with detonation instability (Boisseau et al. 1996; Gamezo et al. 1999) can grow to significant scales.

Alternatively, the detonation could be switched on at a stage in which the deflagration flame has propagated sufficiently close to the low-density part of the expanding white dwarf that the products of detonation bear the imprint of the complex structure of deflagration.

A delayed detonation would be able to boost the outer layers to the velocities we observe. It may also be consistent with the absence of iron features at very high velocity. Detailed modeling is needed in order to understand the clumpy structure of the products of nuclear burning, especially silicon, that these data indicate.

6.3. *Off-centered Delayed Detonation*

According to a different model, which naturally produces a globally aspherical Type Ia is given in Livne (1999) and more recently in 3D calculations by Gamezo et al. (2004), the detonation is triggered at a point off the center of the white dwarf rather than in a spherical shell. The result is that the inner nickel region is offset from the centroid of the density distribution. The resulting off-center production of gamma-ray energy input can induce polarization even in a spherical density distribution (Chugai 1992; Höflich 1995). In addition, the silicon is predicted to be left with a distribution that is displaced from the centroid of the density distribution. This leads naturally to the possibility of a

globally asymmetric silicon distribution that has the potential to produce significant polarization by large-scale blocking of the photosphere as well as smaller scale clumps of silicon resulting from the turbulent burning. This sort of model thus has the capability of producing all the polarized signatures of the silicon-rich layer. Since the photosphere might also be significantly aspherical from the energy input or the asymmetric density distribution, a large continuum polarization may be produced by such a model; this should be confronted with detailed theoretical modeling. This model can be tested by spectroscopic observations in the nebular phase. We defer a detailed discussion of this model to a later paper when the analysis of the complete data set of our observations is undertaken.

6.4. *Gravitationally Confined Detonation*

In the model recently proposed by Plewa et al. (2004), the explosion begins as a deflagration born slightly off center in the white dwarf. Buoyancy dominates the evolution of the deflagration, resulting in a very rapidly rising plume of burned material (see also Livne et al. 2005). This plume displaces the outer (unburned) layers of the star, which propagate ahead of burned bubble material across the surface of the star. This flow converges at the point opposite from where the plume emerges, and the resulting rapid compression of the unburned material triggers a detonation. An advantage of this model is that it may not require triggering the detonation artificially. This model has about 1% of a solar mass of iron group elements on the surface of the white dwarf resulting from the surface flow of the plume material. As for pure deflagration models, detailed spectroscopic modeling is needed to tell whether this amount of iron is allowed by observations. In addition, the requirement of significant preexpansion so that sufficient intermediate-mass elements are produced in the velocity range from 11,000 to 25,000 km s^{-1} to match the observed spectra may further constrain this model. Note that preexpansion is necessary to produce intermediate-mass elements in the outer layers but can significantly weaken the shock of the merging plume matter; this will work against the triggering of the detonation. Therefore, these observations will set limits on the parameter space where this mechanism may work. Due to preexpansion at the stage of detonation, it is also possible that this mechanism will produce highly aspherical chemical structures such that one side (where detonation is triggered) consists of mainly iron-rich material on the outside, whereas the other side (where the burned bubble emerges) consists of mainly of intermediate-mass elements. Depending on which side faces the observer, the target might appear as iron-rich, SN 1991T-like or silicon-rich, SN 2004dt-like; however, the details of these constraints await thorough theoretical models of these data.

7. IMPLICATIONS FOR SUPERNOVA COSMOLOGY

This study illustrates that the nature of Type Ia supernovae is more heterogeneous than is easily revealed by observing methods less telescope time intensive than spectropolarimetry. We have shown that polarimetry provides information that is often strongly complimentary to other observables, and so can provide important discriminants among theoretical models of SN Ia explosions.

In order to make SNe Ia better understood standard candles, it will be essential (1) to obtain enough data to extract the core commonalities from all the individual cases and (2) to find ways of inferring certain special conditions also from low-resolution spectra and photometry, because only they permit SNe to be observed at cosmological distances. If unrecognized subtypes of SNe occur in different proportions at different redshifts or in different environments, supernova cosmology experiments could be severely compromised by such uncertainties.

There are two effects of asymmetry on the observed magnitudes of a supernova. First, asymmetry affects the total integrated light from a supernova in a particular filter, therefore causing a view-angle dependence of distances. Second, asymmetry will cause intrinsic color dispersions that can make the determination of color-excess due to dust in the host galaxy difficult. The second effect can become very important, as errors on color are amplified when extinction corrections are to be applied.

The nature of events like SN 2004dt may require this group to be separated from other supernovae and call for a recalibration of the methods (e.g., Phillips et al. 1999; Wang et al. 2003a) commonly used to derive distances and dust reddening of SN Ia. This supernova may represent a particular subset of SN Ia, along with SN 1984A, SN 1997bp, and SN 2002bo, with especially high-velocity matter for which the explosion mechanism is significantly different than that for their lower velocity counterparts such as SN 1994D.

An association with dusty environments would suggest also that these events are likely to be from younger progenitor stars and that they may be more abundant at higher red shifts than in our local universe. Identifying these events and applying the proper relations for distance calibration is also critical for removing the effects of progenitor evolution.

8. SUMMARY AND DISCUSSION

Spectropolarimetry is a straightforward, powerful diagnostic tool for supernova explosions. Contrary to conventional perceptions that the interpretation of polarimetry data is complicated and heavily model dependent, many important insights on the geometric structure of supernovae ejecta can be derived from diagnostic analyses that do not rely on detailed modeling.

In this study we have presented high-quality spectropolarimetry of the Type Ia SN 2004dt. These data allow us to probe the geometric structure of the ejecta from around 11,000 all the way to about 25,000 km s^{-1}.

SN 2004dt adds to the examples of how these simple diagnostic tools can be applied to well-observed supernovae to study the geometric structure of the ejecta. Spectroscopically, we found that most of the spectral features can be identified with intermediate-mass elements with little or no contributions from iron. From spectropolarimetry, we found the high-velocity regions of SN 2004dt to be highly aspherical, clumpy, and probably turbulent.

The results of this study provide significant constraints on theoretical models of Type Ia explosions. Polarimetry of SN Ia probes the origins of the intrinsic diversity of SN Ia and is important for improving them as precise tools of cosmology.

The authors are grateful to the European Southern Observatory for the generous allocation of observing time. They especially thank the staff of the Paranal Observatory for their competent and never-tiring support of this project in service mode. We are grateful to Weidong Li for sharing photometric data before publications and to Tomesz Plewa for helpful discussions. The research of L. W. is supported in part by the Director, Office of Science, Office of High Energy and Nuclear Physics, of the Department of Energy under contract DE-AC03-76SF000098. This work was performed in part during a visit of L. W. to Purple Mountain Observatory, Nanjing, China. The research of J. C. W. is supported in part by NSF grant AST 04-06740.

REFERENCES

Arnett, D. 1969, ApJ, 157, 1369
Barbon, R., Tijima, T., & Rosina, L. 1989, A&A, 220, 83
Benetti, S., et al. 2004, MNRAS, 348, 261
Boisseau, J. R., Wheeler, J. C., Oran, E. S., & Khokhlov, A. M. 1996, ApJ, 471, L99
Branch, D. 1987, ApJ, 316, L81
Chugai, N. N. 1992, Sov. Astron. Lett., 18, 168
Fisher, A., Branch, D., Hatano, K., & Baron, E. 1999, MNRAS, 304, 67
Gamezo, V. N., Khokhlov, A. M., & Oran, E. S. 2004, Phys. Rev. Lett., 92, 1102
Gamezo, V. N., Khokhlov, A. M., Oran, E. S., Chtchelkanova, A. Y., & Rosenberg, R. O. 2003, Science, 299, 77
Gamezo, V. N., Wheeler, J. C., Khokhlov, A. M., & Oran, E. S. 1999, ApJ, 512, 827
Gerardy, C. L., et al. 2004, ApJ, 607, 391
Goldhaber, G., et al. 2001, ApJ, 558, 359
Hansen, C. J., & Wheeler, J. C. 1969, Ap&SS, 3, 464
———. 1995, ApJ, 440, 821
Höflich, P., Gerardy, C. L., Fesen, R. A., & Sakai, S. 2002, ApJ, 568, 791
Howell, D. A., Höflich, P., Wang, L., & Wheeler, J. C. 2001, ApJ, 556, 302
Jeffery, D., Leibundgut, B., Kirshner, R. P., Benetti, S., Branch, D., & Sonneborn, G. 1992, ApJ, 397, 304
Kasen, D., et al. 2003, ApJ, 593, 788
Khokhlov, A. M. 1991, A&A, 245, 114
Kimeridze, G. N., & Tsvetkov, D. Yu. 1986, Astrofizika, 25, 279
Kirshner, R. P., et al. 1993, ApJ, 415, 589
Knop, R., et al. 2003, ApJ, 598, 102
Leonard, D. C., Filippenko, A. V., Ardila, D. R., & Brotherton, M. S. 2001, ApJ, 553, 861
Leonard, D. C., Weidong, Li, Filippenko, A. V., Foley, R. J., & Chornock, R. 2005, ApJ, 632, 450
Livne, E. 1999, ApJ, 527, L97
Livne, E., Asida, S. M., & Höflich, P. 2005, ApJ, 632, 443
Marion, G. H., Höflich, P., Vacca, W. D., & Wheeler, J. C. 2003, ApJ, 591, 316
Moore, M., & Li, W. 2004, IAU Circ., 8386, 1
Nomoto, K. 1982a, ApJ, 253, 798
Nomoto, K. 1982b, ApJ, 257, 780
Nomoto, K., Sugimoto, D., & Neo, S. 1976, Ap&SS, 39, L37
Nomoto, K., Thielemann, F.-K., & Yokoi, K. 1984, ApJ, 286, 644
Patat, F. 2005, MNRAS, 357, 1161
Patat, F., Benetti, S., Cappellaro, E., Danziger, I. J., Della Valle, M., Mazzali, P. A., & Turatto, M. 1996, MNRAS, 278, 111
Patat, F., Pignata, G., & Benetti, S. 2004, IAU Circ., 8387, 3
Phillips, M. M., Lira, P., Suntzeff, N., B., Schommer, R. A., Hamuy, M., & Maza, J. 1999, AJ, 118, 1766
Plewa, T., Calder, A. C., & Lamb, D. Q. 2004, ApJ, 612, L37
Reinecke, M., Hillebrandt, W., & Niemeyer, J. C. 2002, A&A, 391, 1167
Riess, A. G., Nugent, P. E., Filippenko, A. V., Kirshner, R. P., & Perlmutter, S. 1998, ApJ, 504, 935
Röpke, F. K., Niemeyer, J. C., & Hillebrandt, W. 2003, ApJ, 588, 952
Salvo, M., Schmidt, B., & Wood, P. 2004, IAU Circ., 8387, 2
Wang, L. 2003, in Cosmic Explosions in Three Dimensions: Asymmetries in Supernovae and Gamma-Ray Bursts, ed. P. Höflich, P. Kumar, & J. C. Wheeler (Cambridge: Cambridge Univ. Press), 17
———. 2005, ApJ, 635, L33
Wang, L., Baade, D., Höflich, P., Wheeler, J. C., Kawabata, K., & Nomoto, K. 2004, ApJ, 604, L53
Wang, L., Goldhaber, G., Aldering, G., & Perlmutter, S. 2003a, ApJ, 590, 944
Wang, L., Howell, D. A., Höflich, P., & Wheeler, J. C. 2001, ApJ, 550, 1030
Wang, L., & Hu, J. 1994, Nature, 369, 380
Wang, L., & Wheeler, J. C. 1997, IAU Circ., 6622, 2
Wang, L., Wheeler, J. C., & Hoeflich, P. 1997, ApJ, 476, L27
Wang, L., Wheeler, J. C., Li, Z., & Clocchiatti, A. 1996, ApJ, 467, 435
———. 2002, ApJ, 579, 671
Wang, L., et al. 2003b, ApJ, 591, 1110
Wheeler, J. C., & Harkness, R. P. 1990, Rep. Prog. Phys., 53, 1467
Wheeler, J. C., Höflich, P., Harkness, R. P., & Spyromilio, J. 1998, ApJ, 496, 908
Whelan, J., & Iben, I. J. 1973, ApJ, 186, 1007
Woosley, S. E., & Weaver, T. A. 1994, ApJ, 423, 371
Yamaoka, H., Nomoto, K., Shigeyama, T., & Thielemann, F. 1992, ApJ, 393, L55